Pergamon

Int. J. Multiphase Flow Vol. 23, No. 4, pp. 651–669, 1997

Printed in Great Britain

PII: S0301-9322(97)00006-2

0301-9322/97 $17.00 + 0.00

TEMPORAL PROPERTIES OF DROP BREAKUP IN THE SHEAR BREAKUP REGIME

W.-H. CHOU, L.-P. HSIANG and G. M. FAETH†

Department of Aerospace Engineering, The University of Michigan, Ann Arbor, MI 48109-2118, U.S.A.

(Received 2 June 1996; in revised form 27 January 1997)

Abstract—The temporal properties of drop breakup in the shear breakup regime were studied using pulsed shadowgraphy and holography for shock wave disturbances in air at normal temperature and pressure. Test conditions included Weber numbers of 125–375, Ohnesorge numbers of 0.003–0.040, liquid/gas density ratios of 670–990 and Reynolds numbers of 3000–12000. The size distributions of drops produced by breakup satisfied Simmons' universal root normal distribution function at each instant of time, with Sauter mean diameters independent of surface tension that exhibited transient and quasi-steady regimes as a function of time. The velocity distribution functions of drops produced by breakup were uniform, with mean drop velocities somewhat larger than the velocity of the parent drop and rms drop velocity fluctuations of 30–40% of the mean streamwise velocity of the gas relative to the parent drop, at each instant of time. The rate of liquid removal from the parent drop was correlated reasonably well by a clipped Gaussian function. The measurements showed that shear breakup is not a localized event; instead, it extends over streamwise distances of 0–100 initial drop diameters, which suggests that it should be treated as a rate process, rather than by jump conditions, in some instances. © 1997 Elsevier Science Ltd.

Key Words: drop breakup, drop dynamics, pulsed holography, sprays, atomization

1. INTRODUCTION

The breakup of individual drops, which is often called secondary breakup, is an important fundamental process of sprays. For example, drops formed by breakup of liquid surfaces, which is often called primary breakup, are intrinsically unstable to secondary breakup, while secondary breakup can be the rate controlling process within dense sprays in much the same way that drop vaporization can be the rate controlling process within dilute sprays (Faeth 1990, 1996; Wu *et al.* 1995). Motivated by these observations, the objective of the present investigation was to extend earlier studies of the regimes and outcomes of secondary breakup due to shock-wave disturbances (Hsiang and Faeth 1992, 1993, 1995), to consider the evolution of breakup as a function of time during breakup.

Earlier studies of drop breakup are discussed by Wu *et al.* (1995), Faeth (1990, 1996), Giffen and Muraszew (1953), Hinze (1955), Clift *et al.* (1979), Krzeczkowski (1980) and Wierzba and Takayama (1987, 1988), among others. Shock-wave disturbances were considered during most earlier studies, providing a step change of the ambient environment of the drop, similar to conditions experienced by drops at the end of primary breakup. The main findings of this work included the conditions required for particular deformation and breakup regimes, the times required for the onset and end of breakup, the drag properties of deformed drops, and drop size and velocity distributions at the end of the breakup process (i.e. the jump conditions). An interesting feature of these results is that drop breakup extended over appreciable regions of time and space and was not properly described by jump conditions in some instances. This behavior can be illustrated in terms of the characteristic breakup time, t^*, of Ranger and Nicholls (1968), defined as follows

$$t^* = d_o(\rho_L/\rho_G)^{1/2}/u_o, \qquad [1]$$

†To whom correspondence should be addressed.

where d is the drop diameter, ρ is density, u is steamwise drop velocity relative to the gas, the subscripts L and G denote liquid and gas properties, and the subscript o denotes conditions at the start of breakup. Liang *et al.* (1988) show that breakup times for a wide range of conditions are 5.5 t^*, which is comparable to flow residence times within the dense spray region where secondary breakup is a dominant process (Faeth 1990, 1996; Wu *et al.* 1995). Viewed another way, the original (or parent) drop moves roughly 40 initial drop diameters, while the smallest drops formed by breakup move up to 100 initial drop diameters, during the period of breakup within the shear breakup regime (Hsiang and Faeth 1992, 1993, 1995). Such distances can represent a significant fraction of the length of the dense spray region. These observations suggest that the time-resolved features of secondary breakup eventually must be understood. Thus, the present study seeks to provide some of this information by carrying out new measurements within the shear breakup regime, where breakup proceeds by the stripping of drop liquid from the periphery of the parent drop, because this regime tends to dominate drop breakup in practical sprays (Hsiang and Faeth 1995). Phenomenological theories also were developed to help interpret and correlate the measurements.

The present measurements were carried out using a shock tube facility, with the drop environment approximating air at normal temperature and pressure (NTP). Properties during breakup were observed using pulsed shadowgraphy and holography. Test conditions were limited to relatively large liquid/gas density ratios ($\rho_L/\rho_G > 500$) in order to minimize potential complications due to the inertia of the continuous phase. The test conditions also involved limited ranges of Weber and Ohnesorge numbers, which Hinze (1955) has shown define the boundaries of the shear breakup regime at large liquid/gas density ratios. The Weber number, We, is a measure of the relative importance of drop drag and surface tension forces, and is defined as follows

$$\mathrm{We} = \rho_G d_o u_o^2/\sigma, \qquad [2]$$

where σ is the surface tension of the drop liquid. The Ohnesorge number, Oh, is a measure of the relative importance of liquid viscous forces and surface tension forces, and is defined as follows

$$\mathrm{Oh} = \mu_L/(\rho_L d_o \sigma)^{1/2}, \qquad [3]$$

where μ is the molecular viscosity. The experiments involved relatively small initial Ohnesorge numbers (Oh < 0.04) in order to minimize potential complications due to effects of liquid viscosity. For this range of Oh, operation in the shear breakup regime requires We > 90, in order to exceed the multimode/shear breakup regime transition, and We < 800, in order not to exceed the shear/drop-piercing (or shear/catastrophic) breakup regime transition (Giffen and Muraszew 1953; Hinze 1955; Reinecke and McKay 1969; Reinecke and Waldman 1970). Drop liquids included water, ethyl alcohol and various glycerol mixtures in order to provide information about effects of drop liquid properties.

2. EXPERIMENTAL METHODS

2.1. Apparatus

The test apparatus will be described briefly because it was similar to earlier work (Hsiang and Faeth 1992, 1993, 1995). A shock tube with the driven section open to the atmosphere was used for the measurements. The driven section had a rectangular cross-section (38 mm wide and 64 mm high) and was sized to provide test times of 17–21 ms in the uniform flow region behind the incident shock wave. The test location had quartz windows to allow observations of drop breakup.

A vibrating capillary tube drop generator, similar to the arrangement described by Dabora (1967), was used to generate a stream of drops having a constant diameter. An electrostatic drop selection system, similar to Sangiovanni and Kestin (1977), was used to control the spacing between drops. This drop stream passed vertically across the shock tube at the test location. The spacing between drops was 5–7 mm while drop sizes were ≤ 1 mm; therefore, drops always were present within the region observed while interactions between adjacent drops during shear breakup were negligible.

2.2. *Instrumentation*

Pulsed holography and shadowgraphy were used to observe the properties of the parent drop and the drops produced by breakup as a function of time during breakup. The holocamera used two frequency doubled YAG lasers (Spectra Physics Model GCR-130, 532 nm wavelength, 7 ns pulse duration, up to 300 mJ per pulse) which could be fired with pulse separations as small as 100 ns. An off-axis holocamera arrangement was used with the optics providing a 25 mm diameter field of view at the test drop location. Reconstruction of the double-pulse holograms yielded two images of the spray so that drop velocities could be found given the time of separation between the pulses (which was measured with a digital oscilloscope). The second laser pulse was somewhat weaker than the first, which allowed directional ambiguity to be resolved because stronger pulses yielded sharper reconstructed images. This arrangement also provided shadowgraphy by blocking the reference beam.

The hologram reconstruction system was modified from Hsiang and Faeth (1992, 1993, 1995). A helium–neon laser (Spectra Physics Model 124B, cw laser, 35 mW of optical power) was used to reconstruct the image, which was observed using a CCD camera (Sony, Model XC-77) with optics to yield a magnification of 300:1 and a field of view of the image (on the monitor) of 1.2×1.4 mm. The optical data was obtained using a frame grabber (Data Translation DT 2851) and processed using Media Cybernetics Image-Pro Plus software. Various locations in the hologram reconstruction were observed by traversing the hologram in two directions, and the videocamera of the image display in the third direction. Positions were selected for viewing using stepping motor driven linear traversing systems (Velmex, Model VP9000) having 1 μm positioning accuracies. The combined holocamera/reconstruction system allowed objects as small as 3 μm to be observed and objects as small as 5 μm to be measured with 5% accuracy.

Drop sizes and velocities were measured as described by Hsiang and Faeth (1992, 1993, 1995). Present results were found by summing over at least four realizations, and considering 50–100 liquid elements, in order to provide drop diameter and velocity correlations. These sample sizes were smaller than past studies of jump conditions in order to maintain a manageable test program while resolving drop properties as a function of time. Estimated experimental uncertainties (95% confidence) are less than 15% for drop diameters and less than 20% for streamwise mean drop velocities and rms drop velocity fluctuations; uncertainties of cross-stream mean velocities are larger due to the smaller values of these velocities, as discussed later.

2.3. *Test conditions*

The test conditions are summarized in table 1. The liquid properties were obtained from Lange (1952), except for the surface tensions of the glycerol mixtures which were measured in the same manner as Wu *et al.* (1991). Shock wave Mach numbers in the shock tube were relatively low, less than 1.15; therefore, the physical properties of the gas in the uniform flow region behind the shock wave, where drop breakup occurred, were nearly the same as air at NTP.

The specific range of the present tests is illustrated on the drop deformation and breakup regime map appearing in figure 1. This regime map is extended from Hsiang and Faeth (1995) to include new transitions measured during the present investigation, as follows: the shear/drop-piercing (or catastrophic) breakup regime transition at large We, first observed by Reinecke and McKay (1969), and the more qualitative shear/long-ligament breakup regime transition at large Oh, to be discussed later. Aside from experiments used to define the shear/drop-piercing and shear/long-ligament

Table 1. Summary of the test conditions†

Liquid	ρ_L (kg/m^3)	$\mu_L \times 10^4$ (kg/ms)	σ (mN/m)	d_o (μm)	Oh $\times 10^3$	Re
Water	997	8.94	70.8	590–1000	3.4–4.4	4930–11150
Ethyl alcohol	800	16.0	24.0	780–1000	11.5–13.1	3070–5740
Glycerol (42%)‡	1105	35.0	65.4	1000	13.0	6000–11180
Glycerol (63%)‡	1162	108.0	64.8	1000	39.4	5840–11240

†Air initially at 98.8 kPa and 298 $\pm$ 2 K in the driven section of the shock tube. Shock Mach numbers in the range 1.01–1.15 with We in the range 125–375. Properties of the air were taken at normal temperature and pressure: $\rho_G = 1.18$ kg/m^3, $\mu_G = 18.5 \times 10^{-4}$ kg/ms.

‡Percentage glycerin by mass.

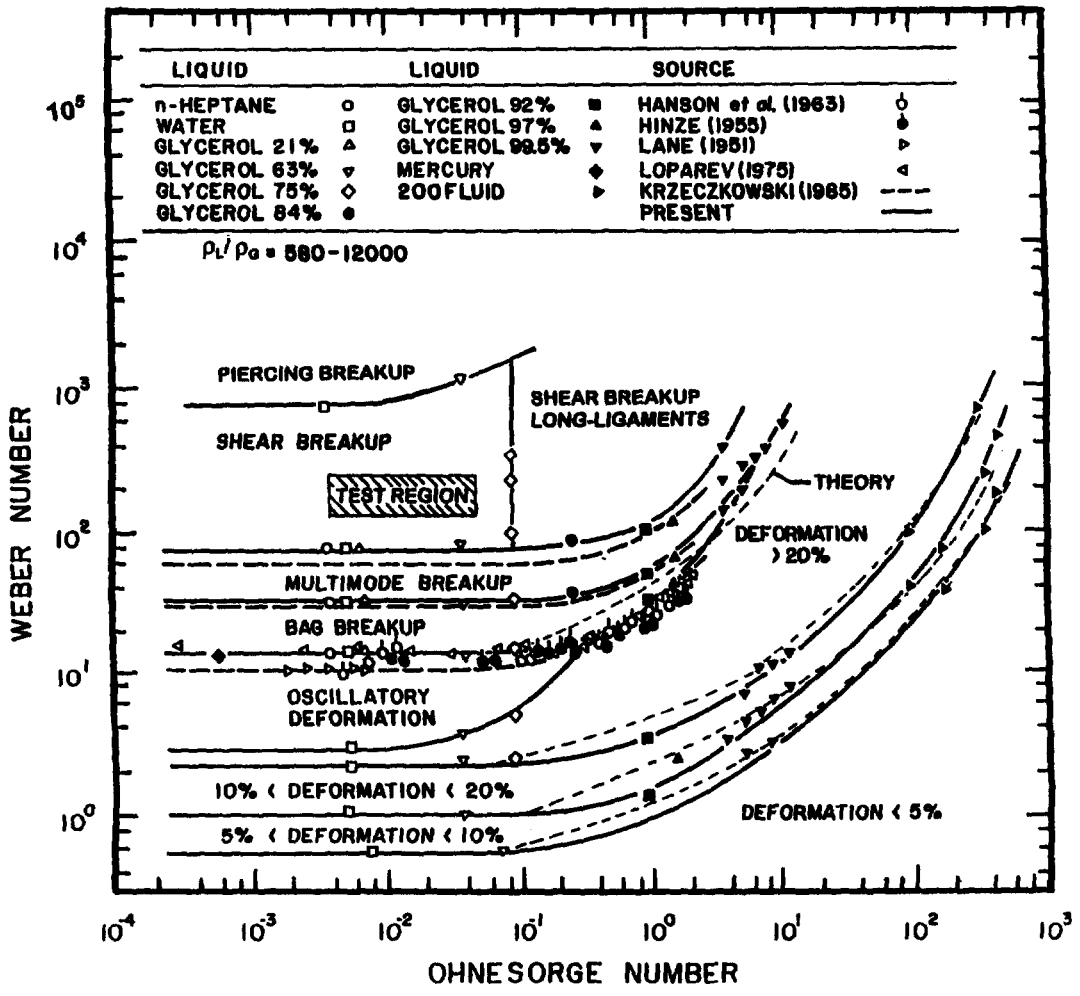

Figure 1. Drop deformation and breakup regime map for shock-wave disturbances, extended from Hsiang and Faeth (1995).

breakup regime transitions, however, present measurements were confined to the cross-hatched region which is conservatively located well within the shear breakup regime at small Ohnesorge numbers. This involved ρ_L/ρ_G of 670–990, We of 125–375 and Oh of 0.003–0.040. The range of initial drop Reynolds numbers, Re, was 3000–12000, where

$$\mathrm{Re} = \rho_G u_o d_o/\mu_G. \qquad [4]$$

These values of Re are higher than conditions where the gas viscosity has a significant effect on drop drag properties, e.g. the drag coefficient, C_D, for spheres only varies in the range 0.4–0.5 for this Reynolds number range (White 1974).

3. RESULTS AND DISCUSSION

3.1. *Flow visualization*

Pulsed shadowgraph flow visualizations provide an overview of the temporal properties of shear breakup. Figure 2 is an illustration of a series of these shadowgraphs for a condition toward the lower Oh values considered during the present study, see figure 1. It should be noted that the onset and end of breakup (where liquid removal from the parent drop begins and ends) occur at t/t^* of roughly 1.5 and 5.5, respectively (Liang *et al.* 1988), for reference purposes. The shock wave, and the flow velocities behind the shock wave, pass from the top to the bottom of the shadowgraphs.

The shadowgraph at $t/t^* = 0$ in figure 2 provides a size reference and illustrates the initial spherical shape of the drop. After passage of the shock wave, the drop deforms into a flattened shape, (see $t/t^* = 1$), because the liquid is drawn toward the drop periphery where the pressure is low due to acceleration of the gas flow over the drop surface. Ligaments and drops begin to be stripped from the drop when $t/t^* = 1.5$ (which is not shown in figure 2); even at $t/t^* = 2$, however, there is an extensive system of ligaments protruding from the periphery of the parent drop, with numerous individual drops present near the downstream end of the ligaments as a result of ligament breakup. Subsequently, the diameter and length of the ligaments, the diameters of the drops produced by breakup of the ligaments, the number of individual drops, and the range of streamwise distances where drops are observed, all increase as t/t^* increases; in contrast, the number of ligaments and the size of the parent drop both decrease as t/t^* increases—compare results at $t/t^* = 2$, 3, 4 and 5. Finally, the diameter of the parent drop, and the gas velocity relative to the parent drop, become small so that drop breakup ends at $t/t^* = 5.5$ (just beyond the range of photographs in figure 2). Subsequently the parent drop evolves toward a spherical shape as its relative velocity continues to decrease.

Increasing Ohnesorge numbers cause the maximum lengths of the ligaments to become progressively larger. This behavior follows from evolution of shear breakup toward large Oh conditions that are dominated by drop deformation and the formation of elongated single drops that are resistant to ligament breakup. Such configurations vastly complicate problems of temporally resolving drop breakup; therefore, present experiments were confined to $\mathrm{Oh} < 0.1$, which was somewhat arbitrarily defined as the onset of the long ligament regime of shear breakup. Figure 3 is an illustration of breakup behavior at the transition condition to the long ligament regime. A series of shadowgraphs at the same values of t/t^* as figure 2 are shown for a glycerol (75% glycerin by mass) drop having $d_o = 1000\ \mu\mathrm{m}$, $\mathrm{We} = 250$ and $\mathrm{Oh} = 0.099$. As before, both shock and flow velocities are directed from the top to the bottom of the shadowgraphs.

The shadowgraphs illustrated in figure 3 are qualitatively similar to those of figure 2. Ligament lengths and the extent of the region containing drops progressively increase, while the size of the parent drop progressively decreases, as t/t^* increases. Tracking and identifying intermediate

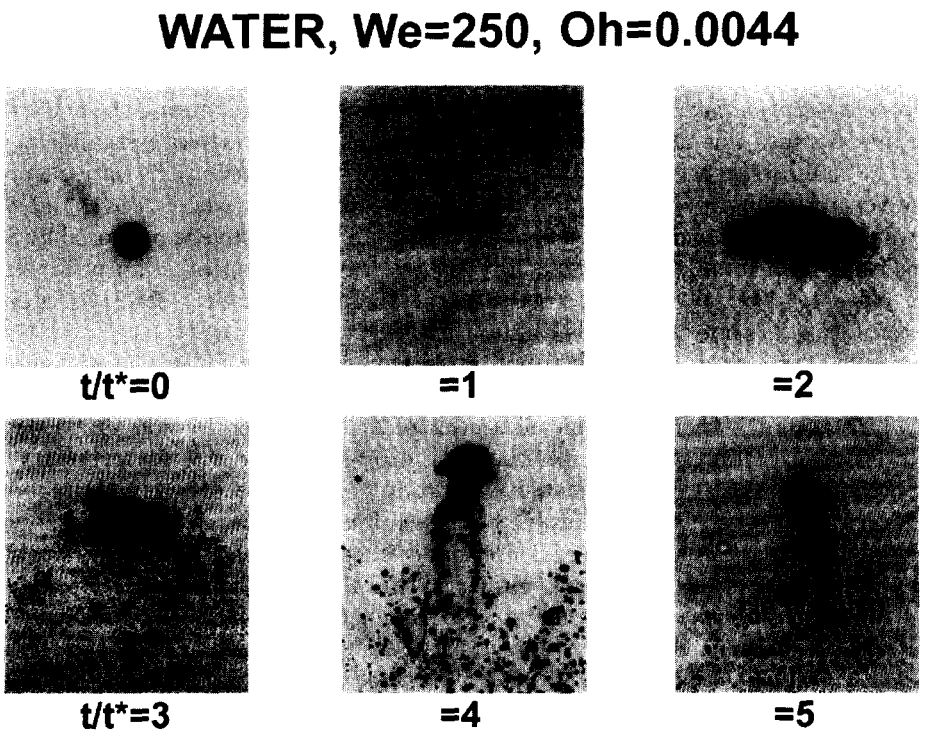

Figure 2. Flash shadowgraphs of the shear breakup of a water drop as a function of time: $d_o = 590\ \mu\mathrm{m}$, $\mathrm{We} = 250$ and $\mathrm{Oh} = 0.0044$.

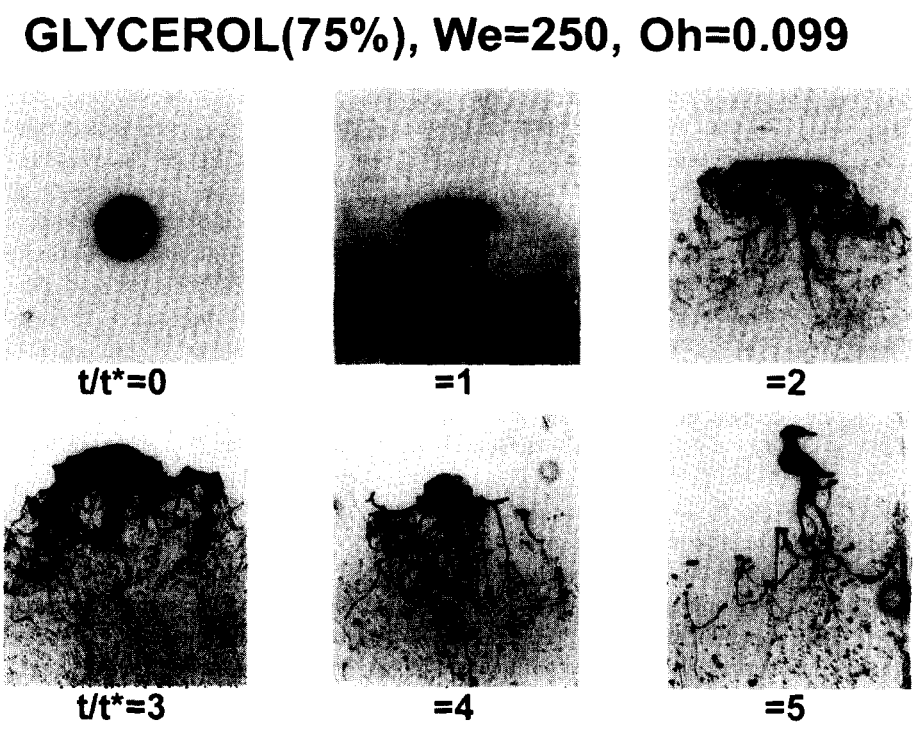

Figure 3. Flash shadowgraphs of the shear breakup of a glycerol drop (75% glycerin by mass) as a function of time: $d_o = 1000\ \mu$m, We = 250 and Oh = 0.099.

breakup points along very long ligaments seen at these conditions, even when using holography, however, is very problematical. Thus, present test conditions were limited to Oh ≤ 0.04 which yielded manageable ligament lengths in a region somewhat below the transition to the long-ligament shear breakup regime.

3.2. Drop sizes

*3.2.1. Drop size distribution.*The evolution of drop size distributions during shear breakup was considered first because this affects the information needed to characterize secondary breakup properties. The main issue was to determine whether drop size distributions varied appreciably from the universal root normal distribution with $MMD/SMD = 1.2$, where MMD and SMD are the mass median and Sauter mean diameters of the distribution, respectively, proposed by Simmons (1977), which has been found to be satisfactory for a variety of drop breakup processes (Faeth 1990, 1996; Wu *et al.* 1995; Hsiang and Faeth 1992, 1993, 1995). See Belz (1973) for a discussion of the properties of the root normal distribution function.

Typical results from the drop size distribution measurements are illustrated in figure 4. The number of drops available to define the drop size distribution for each breakup condition and t/t^* is limited, which accounts for the significant scatter of drop size distribution properties seen in figure 4. Nevertheless, within the scatter of the data, drop sizes produced by secondary breakup are represented reasonably well by the universal root normal size distribution function with $MMD/SMD = 1.2$. This behavior is plausible because primary and secondary breakup processes, as well as drops at various positions within dense sprays, generally satisfy the universal root normal size distribution function, as mentioned earlier. With the two-parameter root normal size distribution function established for the temporal behavior of secondary drop breakup, drop size information can be summarized by the SMD alone (Hsiang and Faeth 1992).

3.2.2. Temporal evolution of the SMD.General description. Correlating expressions for the SMD as a function of time during secondary breakup in the shear breakup regime were sought using methods similar to Hsiang and Faeth (1992) and Wu *et al.* (1991). The present approach was motivated by the flow visualizations illustrated in figures 2 and 3. These results show that ligaments

(which subsequently break up into drops having comparable diameters) are stripped at the periphery of the parent drop from the liquid-phase vortical region (or boundary layer-like flow) that forms along the liquid surface on the upstream (windward) side of the drop during secondary breakup in the shear breakup regime. This behavior also was suggested by earlier work which showed that drop sizes after secondary breakup mainly depend on the viscosity, rather than the surface tension, of the liquid phase (Hsiang and Faeth 1992). In addition, initial measurements during the present investigation also suggested a strong effect of liquid viscosity on the drop sizes produced by secondary breakup. Finally, two basic types of behavior were observed during present experiments, as follows: (1) a regime where there was a progressive increase of ligament diameters, and a corresponding increase of the *SMD* of drops formed from these ligaments, as a function of time during breakup, which was mainly seen when the liquid viscosity and the time after the start of breakup were both small (this behavior is best characterized by the flow visualization of figure 2); and (2) a regime where the ligament diameters, and the SMD of drops formed from these ligaments, were relatively independent of time, which was mainly seen when the liquid viscosity and the time after the start of breakup were both large (this behavior is best characterized by the flow visualization of figure 3). Thus, liquid viscosity had an important effect on drop sizes even though all test conditions involved sufficiently small Ohnesorge numbers so that variations of liquid viscosity did not affect criteria for the onset of breakup, see figure 1. Both of these behaviors suggest that vorticity within the parent drop affects breakup; therefore, these effects will be considered similar to past study of drop size jump conditions due to Hsiang and Faeth (1992).

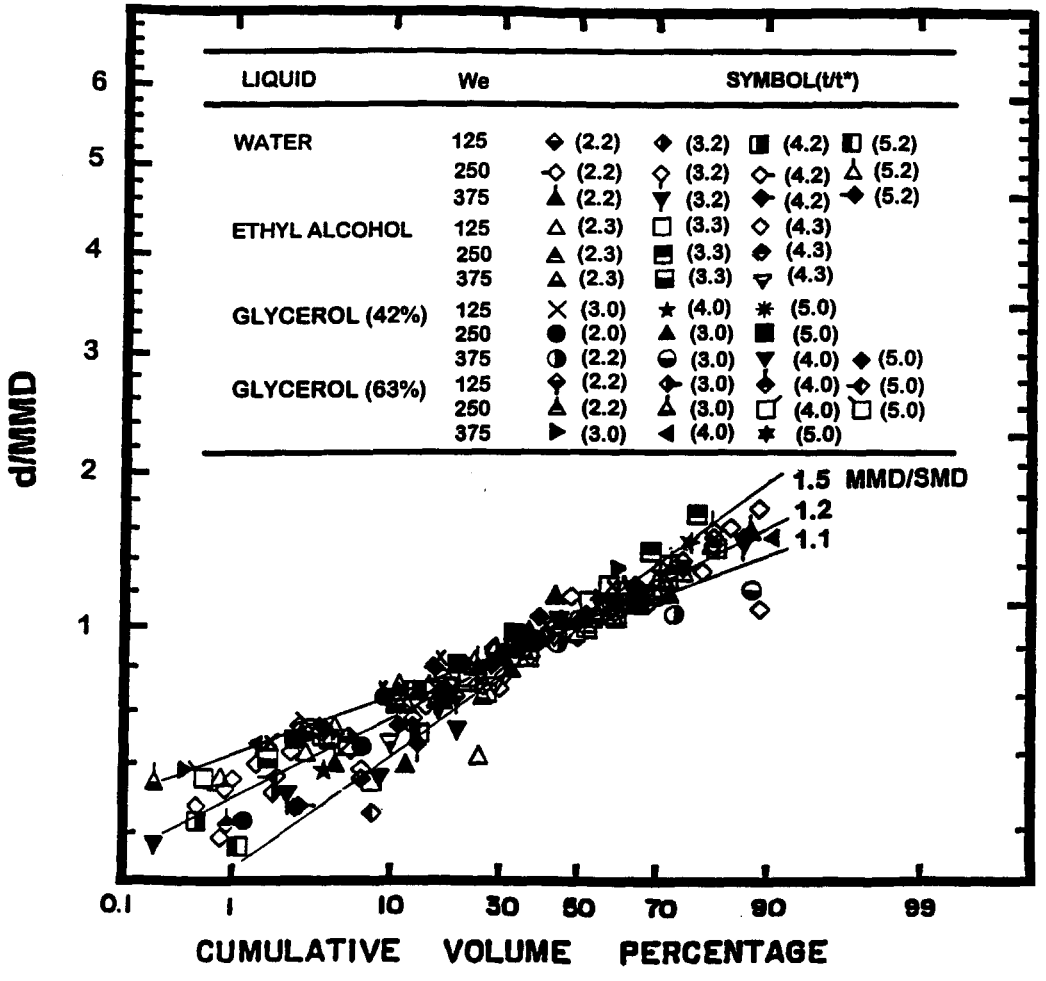

Figure 4. Diameter distribution of drops produced by shear breakup plotted according to the root normal distribution function.

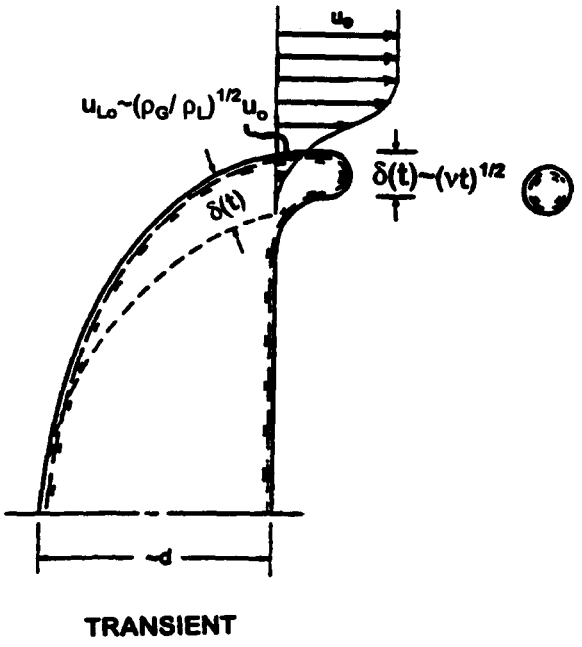

Figure 5. Sketch of the transient shear breakup mechanism at small Ohnesorge numbers ($t/t_c \leq 1$).

The phenomenological analyses to find the temporal variation of drop sizes during secondary breakup are based on the flow configurations appearing in figures 5 and 6. Both figures are sketches of the parent drop after the deformation period, when drops are being formed from the periphery of the parent drop. It is assumed that drops are formed from the vortical region in the liquid (or liquid boundary layer) that develops on the upstream side of the drop, that this layer is laminar, and that the thickness of this layer near the drop periphery, $\delta(t)$, is proportional to the *SMD* of

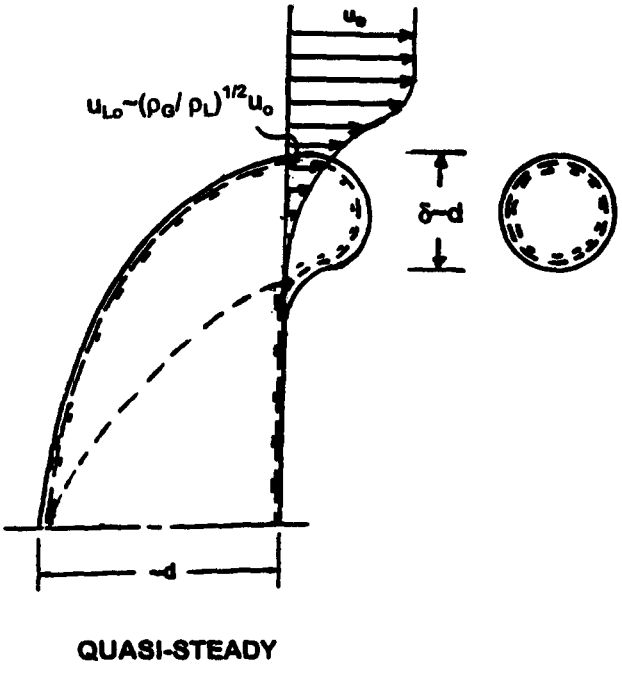

Figure 6. Sketch of the quasi-steady shear breakup mechanism at small Ohnesorge numbers ($t/t_c \geq 1$).

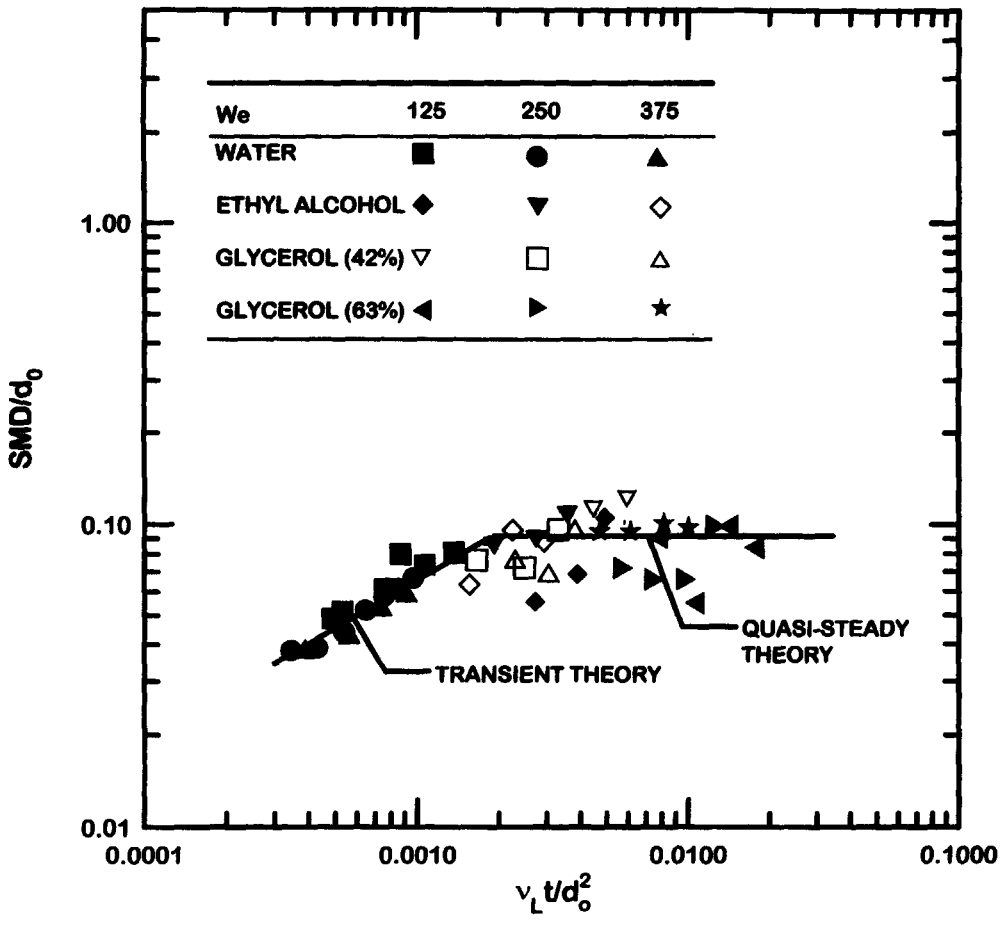

Figure 7. Temporal variation of the *SMD* of drops produced by shear breakup.

the drops currently being formed by shear breakup, similar to earlier considerations of jump conditions to find drop sizes after shear breakup due to Hsiang and Faeth (1992). Then, the two types of behavior noted earlier represent different states of the transient development of the vortical region, which will be denoted the transient and quasi-steady shear breakup regimes in the following. In order to fix ideas, the transition between the transient and quasi-steady shear breakup regimes will be assumed to occur at a time t_c to be quantified later.

Transient shear breakup. The transient breakup mechanism is illustrated in figure 5. This regime is observed at short times after the start of breakup, particularly for liquids that have a small viscosity so that the temporal rate of growth of the thickness of the boundary layer on the windward side of the drop is relatively slow. Then the thickness of the boundary layer, normalized by the initial boundary layer thickness, can be expressed as follows (Schlichting 1975)

$$\delta(t)/d_o = C_t(\nu_L t/d_o^2)^{1/2},\ t/t_c < 1, \qquad [5]$$

where ν_L is the kinematic viscosity of the drop liquid and C_t is an empirical constant on the order of unity. Assuming $SMD(t) \sim \delta(t)$, an equation for the temporal variation of drop sizes in the transient shear breakup regime can be obtained from [5], as follows

$$SMD(t)/d_o = C_s C_t(\nu_L t/d_o^2)^{1/2},\ t/t_c < 1, \qquad [6]$$

where C_s is another empirical constant on the order of unity.

Present measurements of $SMD(t)$ are correlated in terms of [6] for the transient shear breakup regime in figure 7. At small values of $\nu_L t/d_o^2$, the measurements exhibit an excellent correlation

according to the transient theory of [6]; the corresponding theoretical correlation, involving a least-squares fit based on [6] while maintaining the square root dependence of $(v_L t/d_o^2)$, is as follows

$$SMD(t)/d_o = 2.0(v_L t/d_o^2)^{1/2},\ t/t_c < 1. \quad [7]$$

The best fit expression of [7] is also plotted in figure. 7. Limiting the data used to correlate [7] to $v_L t/d_o^2 < 0.00020$, yields a standard deviation of the coefficient on the right hand side of [7] of 13%, with the correlation coefficient of the fit being 0.96. If the power of $(v_L t/d_o^2)$ in [7] is found from a least-squares fit of the same data set, a value of 0.57 with a standard deviation of 0.04 is obtained, which is not statistically different from the 1/2 power based on the phenomenological theory used in [7]. In addition, the coefficient on the right hand side of [7] has an order of magnitude of unity as anticipated.

The experimental results illustrated in figure 7 exhibit a transition from the transient regime for values of $v_L t/d_o^2 > 0.0020$, which will be taken to represent conditions in the quasi-steady shear breakup regime in the following, as denoted on the figure. This transition completes the definition of t_c, which can be expressed as follows

$$t_c/t^* = 0.002(\rho_G/\rho_L)^{1/2} u_o d_o/v_L. \quad [8]$$

Based on approximate conservation of momentum scaling, a characteristic initial liquid phase velocity, u_{Lo}, can be defined as $\rho_L u_{Lo}^2 = \rho_G u_o^2$; therefore, the factor on the right-hand side of [8] can be recognized as a characteristic initial liquid phase Reynolds number based on this velocity, i.e. $Re_L = u_{Lo} d_o/v_L$. Then, noting that the breakup period ends when $t/t^* = 5.5$ from Liang *et al.* (1988), [8] implies that transient behavior will be observed for the entire breakup process when $Re_L > 2750$. For present tests, such conditions were encountered for water drops having We = 250 and 375. At the other extreme, present measurements for ethyl alcohol and glycerol drops were mainly in the quasi-steady shear breakup regime.

The consistency of [7] with the earlier measurements of Hsiang and Faeth (1992) of the SMD at the end of shear breakup (or the jump conditions) for experiments dominated by large We and low viscosity liquids (which implies behavior mainly in the transient shear breakup regime) is also of interest. In particular, this relationship can be examined by assuming that drop sizes at the end of breakup are dominated by the largest drop sizes produced by breakup which also are generated at the end of breakup where $t = t_b = 5.5t^*$. Then, introducing [1] for t^* into [7] yields the following expression for SMD_e, the SMD for the entire secondary breakup process

$$SMD_e/d_o = 2C_e(t_b/t^*)^{1/2}(\rho_L/\rho_G)^{1/4}[v_L/(d_o u_o)]^{1/2} \quad [9]$$

where C_e is an empirical factor to correct for the fact that jump conditions for drop sizes involve the entire breakup process, and the contribution of the remaining parent drop, rather than just the size of drops produced at the end of shear breakup. Nevertheless, [9] becomes identical to the jump conditions of Hsiang and Faeth (1992) if $2C_e(t_b/t^*)^{1/2} = 6.2$. Recalling that $t_b/t^* = 5.5$, implies that $C_e = 1.3$, which is a value on the order of unity as expected. Thus, present findings for the evolution of SMD as a function of time during shear breakup are consistent with the jump conditions found by Hsiang and Faeth (1992) for secondary breakup in the shear breakup regime.

An interesting feature of both [7] for $SMD(t)$ and [9] for SMD_e is that neither result depends on the surface tension, and thus We, even though conditions required for the appearance of the shear breakup regime at low Oh and large ρ_L/ρ_G are controlled by We, and thus σ. In a sense, this behavior is analogous to the role of Reynolds numbers for turbulent mixing, where the presence of turbulent mixing for jets, wakes, etc. depends on the Reynolds number of the flow, even though the rate of mixing itself is essentially independent of the Reynolds number once the flow is turbulent.

Similar to the correlation of SMD_e of Hsiang and Faeth (1992), [7] can be put into a form emphasizing the Weber number of drops produced by secondary breakup, as follows

$$\rho_G SMD(t) u_o^2/\sigma = 2(t/t^*)^{1/2} We/Re_L^{1/2},\ t/t_c < 1, \quad [10]$$

where the left-hand side of [10] can be recognized as the Weber number of drops formed by secondary breakup based on the SMD and the initial relative velocity. Then, similar to previous considerations of the jump conditions to yield SMD_e (Hsiang and Faeth 1992, 1993), [10] shows

that the Weber number based on $SMD(t)$ and u_o can exceed values of We needed to initiate secondary breakup by shock-wave disturbances. As discussed by Hsiang and Faeth (1993, 1995), however, subsequent tertiary breakup does not occur because these drops have had time to adjust to the disturbance and are subject to different criteria for breakup in addition to effects of reduced relative velocities compared to u_o. Finally, even though [10] involves surface tension, it should be recalled that the surface tension only affects requirements for the onset of secondary breakup regimes for present conditions, while drop sizes produced by secondary shear breakup are independent of surface tension, see [7]–[9].

Quasi-steady shear breakup. The next issue that must be addressed with respect to the temporal evolution of SMD during shear breakup involves behavior in the quasi-steady shear breakup regime. There are two main possibilities for defining behavior in the quasi-steady shear breakup regime, as follows: (1) stabilization of the flow within the drop at the end of the transient period implies $\delta \sim d$, relatively independent of properties like Re_L, as illustrated in figure 6; and (2) complete development of the boundary layer near the surface of the liquid on the windward side of the drop yields δ proportional to the thickness of this boundary layer near the drop periphery, along the lines of the analysis of Hsiang and Faeth (1992). The somewhat increased scatter of the data for the quasi-steady shear breakup regime illustrated in figure 7 suggests the potential for complications due to contributions from both these limits; nevertheless, based on this information, it is reasonable to accept the approach illustrated in figure 6 for the quasi-steady shear breakup regime and adopt the approximation $SMD(t) \sim d_o$ to yield

$$SMD(t)/d_o = 0.09,\ t/t_c > 1, \qquad [11]$$

which is illustrated on the plot. Limiting the data used to correlate [11] to $t/t_c > 1$, or $\nu_L t/d_o^2 > 0.0020$, yields a standard deviation of the coefficient on the right hand side of [11] of 22%, with the correlation coefficient of the fit being 0.91. If the power of $\nu_L t/d_o^2$ in [11] is found from a least-squares fit using the same data set, a value of -0.06 with a standard deviation of 0.10 is obtained, which is not statistically different from the power of zero based on the phenomenological description of [11].

It is also of interest to compare the approximation $\delta \sim d$ used to find [11] with estimates of the thickness of the boundary layer formed near the surface of the liquid on the windward side of the drop. For flows typical of the interior of drops this boundary layer is laminar and its thickness was estimated as the characteristic thickness of a laminar boundary layer on a flat plate having an ambient velocity of u_{Lo} and a length d_o, which implies (Schlichting 1975)

$$\delta(d_o)/d_o = 4.0/[(\rho_G/\rho_L)^{1/2} u_o d_o/\nu_L]^{1/2}. \qquad [12]$$

The values of $\delta(d_o)/d_o$ computed from [12] for present test conditions are summarized in table 2. The tabulation indicates that for measurements involving the quasi-steady shear breakup regime (e.g. alcohol and glycerol drops), $\delta(d_o)/d_o$ from [12] was generally larger than SMD/d_o from [11] and much more variable than the range of SMD/d_o seen in figure 7 for these liquids. In contrast, only results for water drops, which generally did not reach quasi-steady conditions, yield boundary layer thicknesses less than the estimate of [10], which is also consistent with the behavior seen in figure 7. Taken together, these results support the present phenomenological approach where the transient regime ends when the thickness of the vortical region reaches a fraction of the parent drop diameter, as a result of the confined internal flow configuration of the deformed parent drop. Naturally, this limit does not yield formulas for the jump conditions for SMD that are consistent with the earlier results of Hsiang and Faeth (1992), similar to the transient shear breakup regime.

Table 2. Summary of quasi-steady liquid boundary layer thicknesses $(\delta(d_o)/d_o)$†

	Drop liquid			
We	Water	Ethyl alcohol	Glycerol (42%)	Glycerol (68%)
125	0.079	0.137	0.154	0.237
250	0.067	0.115	0.115	0.200
375	0.060	0.104	0.110	0.180

†Estimated from [11].

As mentioned earlier, however, this behavior is not surprising because the measurements of Hsiang and Faeth (1992) were dominated by results from the transient shear breakup regime. Another factor is that drop sizes toward the end of the transient shear breakup regime are comparable to those in the quasi-steady breakup regime, see figure 7; therefore, both sets of results tend to correlate in a similar manner.

3.3. Parent drop velocities

The temporal behavior of the velocity distributions of drops produced by shear breakup is closely associated with the temporal behavior of the velocity of the parent drop; therefore, this issue will be considered first. A correlating expression for the velocity of the parent drop with time was based on the phenomenological analysis of Hsiang and Faeth (1993). The major assumptions of this analysis are as follows: virtual mass, Bassett history and gravitational forces ignored; gas velocities assumed to be constant; mass removal from the parent drop ignored; and constant average drag coefficient assumed over the period of breakup. For present conditions, virtual mass and Bassett history forces are small due to the large values of ρ_L/ρ_G of the flow (Faeth 1990). Similarly, gravitational forces were not a factor because drop motion was nearly horizontal and drag forces were much larger than gravitational forces. In addition, uniform gas properties were a condition of the present experiments. In contrast, the uniform parent drop size approximation was not really justified for present conditions because parent drop diameters at the end of breakup were only 12–30% of the original drop diameters and vary considerably over the period of breakup (Hsiang and Faeth 1993). Nevertheless, accounting for these changes by adopting the original drop diameter and selecting a mean drag coefficient, $\overline{C_D}$, to best fit the measurements yielded reasonably good results in the past (Hsiang and Faeth 1993), and was continued during the present study.

The analysis to find parent drop velocities in a laboratory reference frame, u_p, as a function of time under the preceding approximations is presented by Hsiang and Faeth (1993). These results can be placed in the following form

$$(u_p - u_{p_o})/(u_G - u_{p_o}) = 3\overline{C_D}(t/(4t^*))/(\rho_G/\rho_L)^{1/2}, \qquad [13]$$

where for present conditions $u_{p_o} = 0$ and u_G is the gas velocity in a laboratory reference frame. Earlier evaluation of parent drop velocities at the end of secondary breakup yielded a best fit value of $\overline{C_D} = 5$ in [13] (Hsiang and Faeth 1993).

Measurements of parent drop velocities for various secondary breakup conditions, and times during secondary breakup, were obtained from both the present investigation and from the earlier work of Hsiang and Faeth (1993). These results are plotted according to [13] in figure 8. A best-fit correlation according to [13] also is shown on the figure. The comparison between the measurements and the correlation is seen to be quite good in spite of the approximations of the simplified analysis. This yields the same best-fit value $\overline{C_D} = 5.0$, as the results found earlier by Hsiang and Faeth (1993), with an experimental uncertainty (95% confidence) of the fit of 15%.

3.4. Drop velocity distributions

Mean velocities. The velocity distributions of drops produced by shear breakup were measured as a function of time for all test conditions. It was found that the velocities of drops produced by secondary breakup, relative to the velocity of the parent drop, were related to the characteristic velocity of the liquid at each instant of time, i.e. $(\rho_G/\rho_L)^{1/2}(u_G - u_p)$. In addition, it was found that drop velocities were relatively independent of drop size, i.e. the drop velocity distributions were nearly uniform. Thus, volume-averaged mean streamwise and cross-stream velocities for shear breakup, u_L and v_L, normalized by the characteristic liquid velocity, are plotted as a function of t/t^* in figure 9. Similar to the drop diameters illustrated in figure 7, there is appreciable scatter of the drop velocities in figure 9. This behavior comes about because relatively few drops are available to find appropriate average drop velocities for a given breakup condition and time. In addition, random motions of the ligaments and the parent drop, see figures 2 and 3, yield turbulent-like velocity variations that cause corresponding variations of mean velocities. Nevertheless, it is evident that the mean volume-averaged streamwise and cross-stream velocities

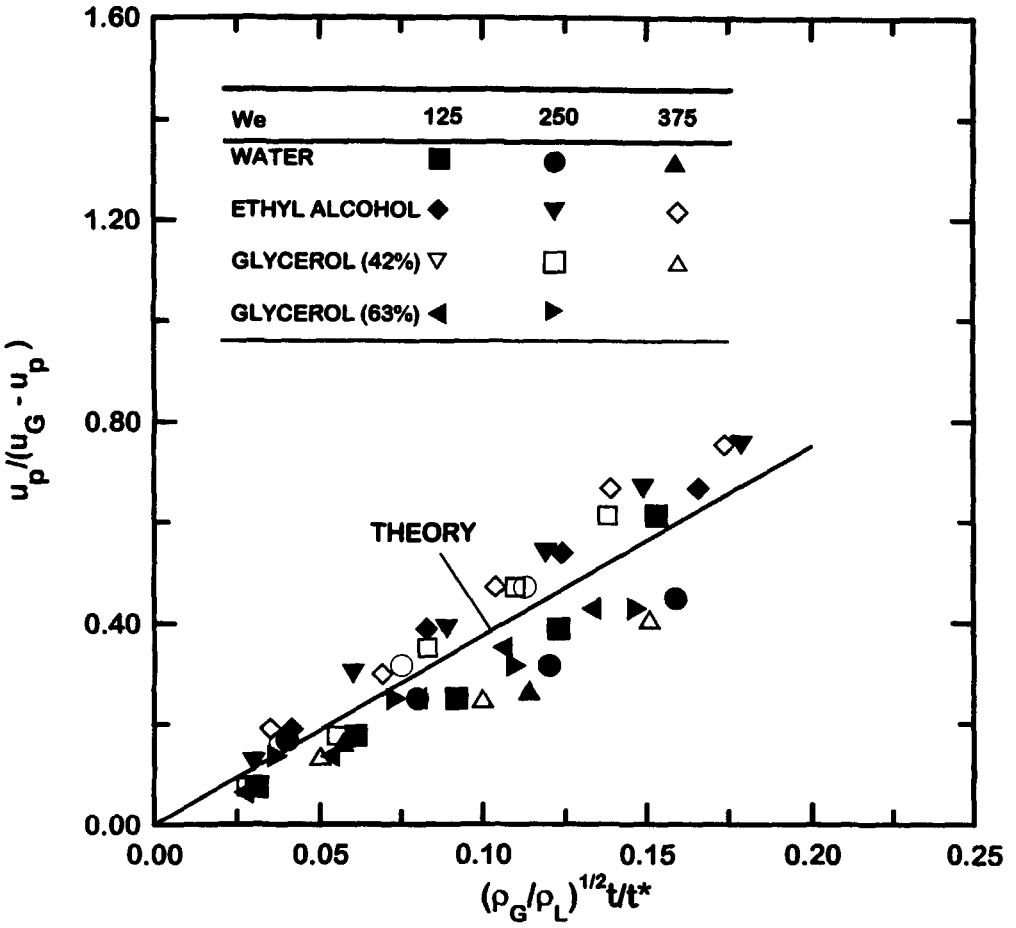

Figure 8. Streamwise velocities of the parent drop as a function of time during shear breakup.

are relatively independent of time as well as drop size and can be correlated reasonably well, as follows

$$(\rho_L/\rho_G)^{1/2}(\bar{u_L} - u_p)/(u_G - u_p) = 9.5 \quad [14]$$

and

$$(\rho_L/\rho_G)^{1/2}\bar{v_L}/(u_G - u_p) = 0 \quad [15]$$

with a standard deviation of the constant on the right-hand side of [14] of 28%. The corresponding standard deviation of the constant on the right hand side of [15] is 4.7; therefore, the mean value of v_L is not statistically different from zero. A difficulty with the correlation of streamwise velocity in [14] is that the actual value of the relative velocity increase of the drops produced by shear breakup is not easily compared with the relative velocity of the parent drop due to the effect of the density ratio. Thus, correlating the streamwise velocity data directly in terms of velocities relative to the velocity of the parent drop yields

$$(\bar{u_L} - u_p)/(u_G - u_p) = 0.37 \quad [16]$$

with the standard deviation of the constant on the right-hand side of [16] of 0.08. This result suggests that there is appreciable acceleration of the drop liquid during breakup, mainly as a result of acceleration of the liquid in the vortical layer near the surface of the parent drop as well as acceleration of liquid in the ligaments prior to final breakup into drops. The relatively large variations of v_L seen in figure 9 certainly tend to support significant effects of liquid acceleration in the ligaments. The corresponding values for v_L yield $v_L/(u_G - u_p) = -0.01$ with a standard deviation of 0.15, which implies that mean radial velocities are not statistically different from zero, as before.

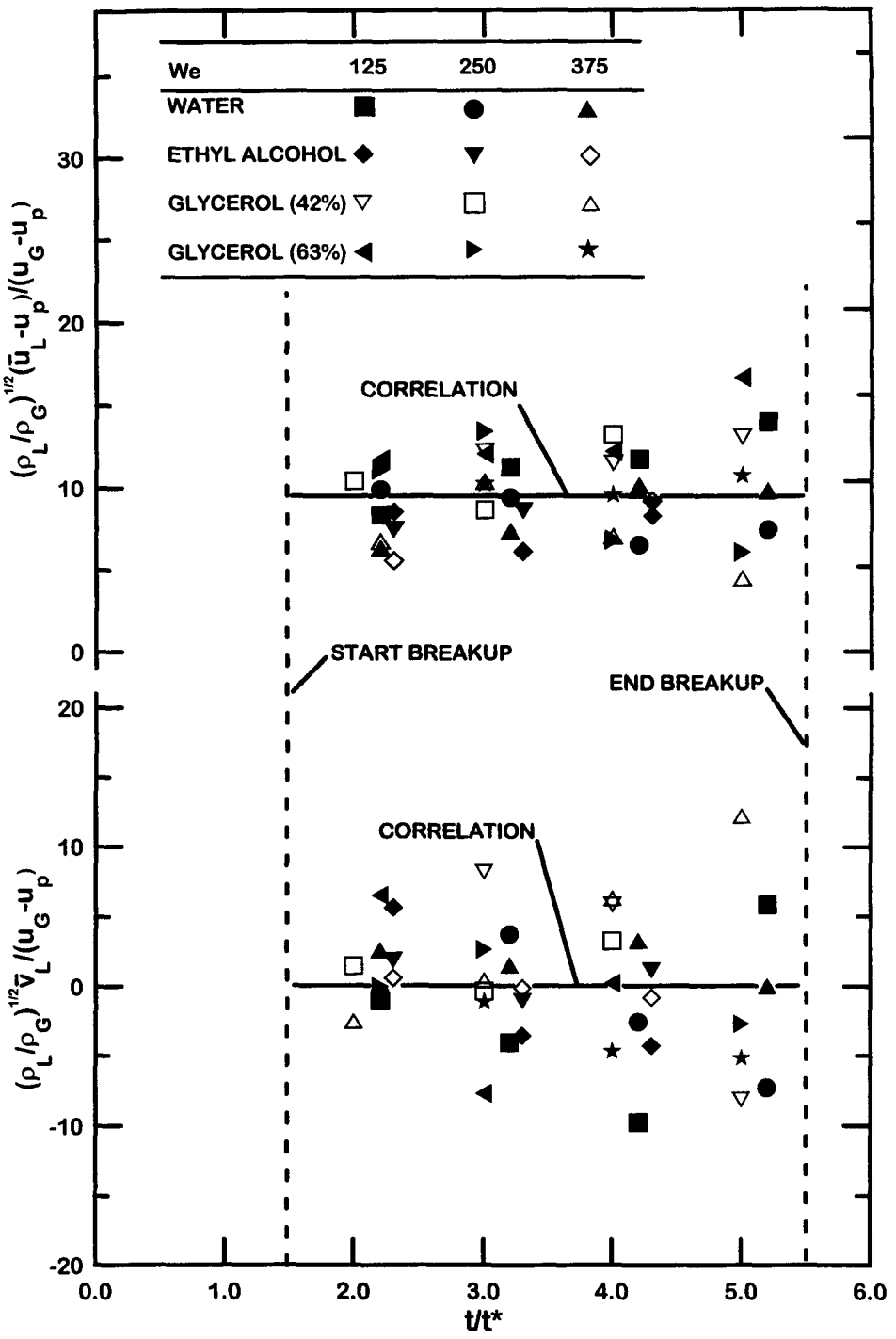

Figure 9. Streamwise and cross-stream mean velocities of drops produced by shear breakup as a function of time during breakup.

The behavior of drop velocities as the drops are formed as a function of time, given by [14] and [15], is in marked contrast to the drop velocity distribution as a function of drop size at the end of breakup (the jump conditions) discussed by Hsiang and Faeth (1993, 1995). For the jump conditions, drop velocities relative to the gas became progressively smaller as the drop sizes become smaller, rather than remaining constant compared to the relative velocity of the gas with respect to the parent drop, similar to the results illustrated in figure 9. This behavior comes about because the characteristic relaxation times of small drops are smaller than those of large drops (Hsiang and

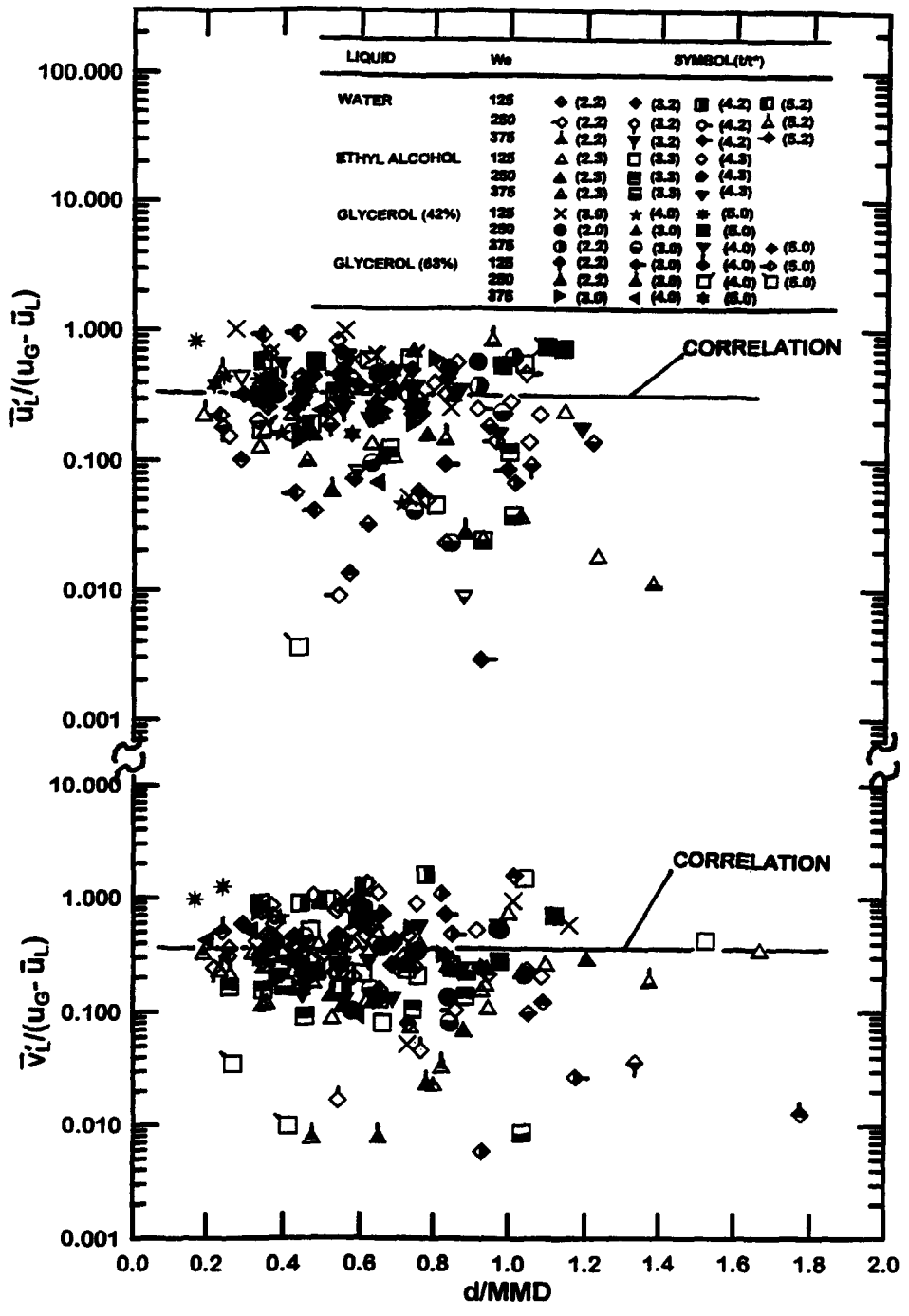

Figure 10. Streamwise and cross-stream rms velocity fluctuations of drops produced by shear breakup as a function of drop size.

Faeth 1992); therefore, small drops undergo a greater acceleration after they are formed than large drops, and more closely approach the gas velocity as a result.

Velocity fluctuations. Volume-averaged rms streamwise and cross-stream velocity fluctuations, $\overline{u_L'}$ and $\overline{v_L'}$ are plotted as a function of d/MMD, with We and t/t^* as parameters, in figure 10. Individual data points on this figure exhibit significant scatter, mainly because each test condition involves a limited number of test drops. Nevertheless, effects of drop size, We and t/t^* appear to be small over the entire data set, when volume-averaged fluctuations are normalized by the mean streamwise

velocity of the drops relative to the gas. The resulting volume-averaged rms streamwise and cross-stream drop velocity fluctuations can be summarized, as follows

$$\overline{u'_L}/(u_G - \overline{u_L}) = 0.31 \quad [17]$$

and

$$\overline{v'_L}/(u_G - \overline{u_L}) = 0.37, \quad [18]$$

where the standard deviations of the numbers on the right-hand sides of these equations are 22%. In view of these uncertainties, the magnitudes of u'_L and v'_L are not statistically different. Taking the data sets as a whole, however, the large number of total samples available to find u'_L and v'_L reduce the experimental uncertainties of these estimates (95% confidence) to less than 10%.

3.5. Drop formation rates

Drop formation rates were estimated using a simplified analysis. This involved the following major assumptions: liquid removal rates were proportional to the thickness of the boundary layer in the liquid on the upstream surface of the drop; liquid removal rates were proportional to the velocity of the drops formed relative to the velocity of the parent drop, estimated from [14]; liquid removal rates were proportional to the perimeter of the drop at its periphery; and breakup begins and ends at $t/t^* = 1.5$ and 5.5, respectively, as determined by Liang *et al.* (1988). The resulting formulation for the rate of production of dispersed liquid drops by secondary breakup, for the transient and quasi-steady drop breakup regimes, is relatively complex. It was noted, however, that the amount of liquid removed from the drop could be approximated by a clipped Gaussian function which simplifies the treatment of the onset and end of secondary breakup. Thus, only the simplified approach will be presented here because it should be useful for detailed analysis of drop breakup processes.

Present measurements of the cumulative volume of liquid removed from the parent drop as a function of time are plotted in figure 11. These results include all test conditions considered during the present investigation. The best-fit correlation of these results, according to a clipped Gaussian function, also is shown on the plot. It is evident that the clipped Gaussian function provides a good fit of the cumulative loss of volume of the parent drop as a function of t/t^*. This formula also provides a reasonably good fit of the rate of removal of drop liquid from the parent drop, except for the singular points at the beginning and end of the period where drop mass is being removed.

The results illustrated in figure 11 can be correlated to provide the mass rate of formation of dispersed drops due to shear breakup, $\dot{m}_p$, normalized by the initial drop mass and t^*, as follows

$$6\dot{m}_p t^*/(\pi\rho_L d_0^3) = 0.42\exp\{0.8(t/t^* - 3.5)^2\}, \ 1.5 \le t/t^* \le 5.5. \quad [19]$$

3.6. Extent of drop-containing region

The region in the streamwise direction that contains drops will be considered in the following in order to provide information needed to evaluate when secondary breakup should be treated as a rate process rather than by jump conditions. This information can be summarized most compactly by plotting the boundaries of the drop-containing region in the streamwise direction, normalized by the initial drop diameter, as a function of t/t^*, based on mean relative velocities only. These boundaries are given by the motion of the parent drop, and the motion of the smallest drop formed at the onset of breakup. Thus, it is evident that these boundaries are fixed by the motion of the parent drop whose velocity is given by [13]. Based on this result, recalling that C_D was found to be a constant for present test conditions, it is evident that ρ_L/ρ_G is the only parameter of the problem. Thus, the sizes of the drop-containing region were found for $\rho_L/\rho_G = 500$ and 1000, which bound the range of conditions considered during the present investigation.

The growth of the spray-containing region in terms of distance in the streamwise direction, x, is plotted as a function of t/t^* in figure 12. Results are shown for the two different values of ρ_L/ρ_G that bound the present measurements, with the limiting values of t/t^* at the onset and end of drop breakup marked on the plot for reference purposes. The span of the drop-containing region increases with both the liquid/gas density ratio and time. For example, the drop-containing region at the end of breakup is in the range $x/d = 40$–120 for $\rho_L/\rho_G = 1000$ but only $x/d = 38$–85 for

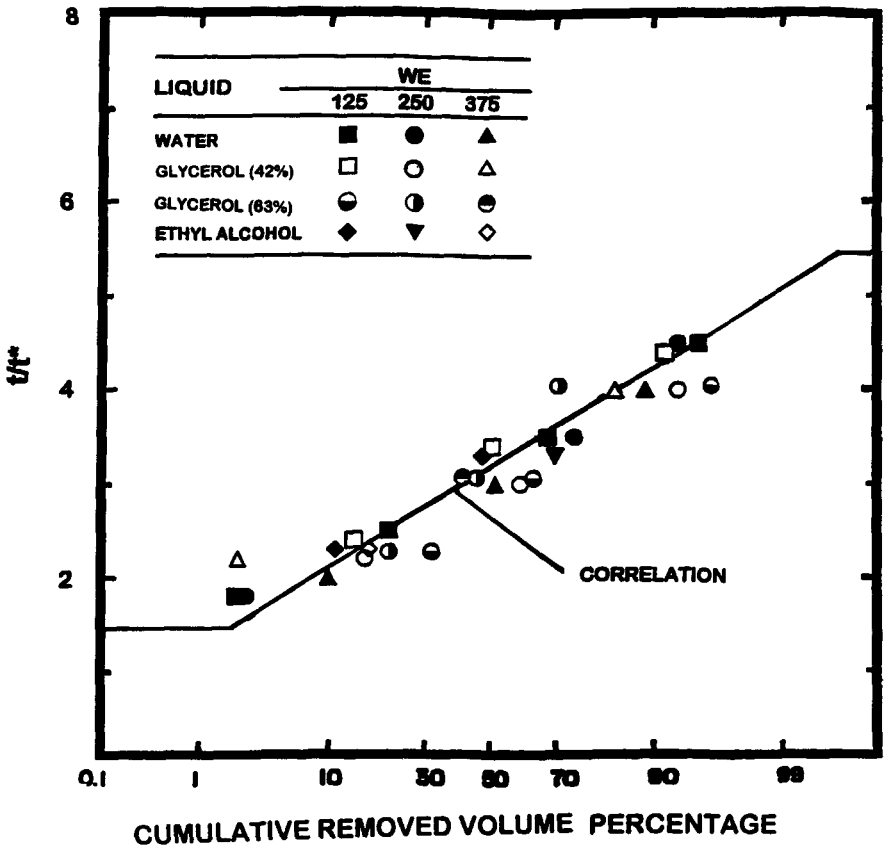

Figure 11. Degree of mass removal from the parent drop as a function of time during shear breakup.

$\rho_L/\rho_G = 500$. Similarly, the mean drop-containing region increases from zero at $t/t^* = 1.5$ to roughly $x/d = 40$–100 at $t/t^* = 5.5$. As noted earlier, the span of the secondary breakup times, the distance traveled by the parent drop, and the span of streamwise distances where drops are present at the end of breakup can be significant in some instances. In such cases, the information found during the present investigation about the temporal evolution of the sizes and velocities of drops produced by secondary breakup, as well as the rate of liquid removal from the parent drop during secondary breakup, should be helpful.

4. CONCLUSIONS

The properties of drop breakup in the shear breakup regime were studied as a function of time for shock-wave disturbances in air at NTP, for the test conditions summarized in table 1. The major conclusions of the study are as follows:

(1) The maximum lengths of ligaments protruding from the periphery of the drops progressively increase with increasing Ohnesorge number causing transition to a long-ligament shear breakup regime at Oh ≈ 0.1; present results are limited to the conventional shear breakup regime at small Ohnesorge numbers (Oh < 0.1).

(2) Drops produced by shear breakup at small Ohnesorge numbers satisfy the universal root normal drop size distribution function with $MMD/SMD = 1.2$, of Simmons (1977), at each instant of time.

(3) The SMD of drops produced by shear breakup at small Ohnesorge numbers exhibit transient and quasi-steady regimes as a function of time, based on the development of the liquid boundary layer within the parent drop; this behavior was correlated based on a phenomenological analysis

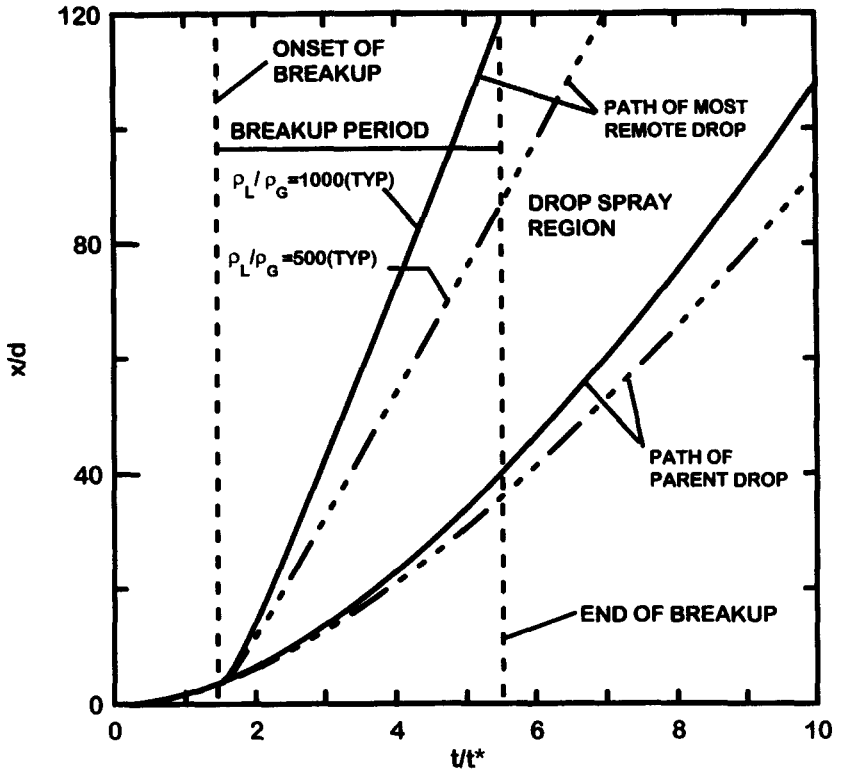

Figure 12. Growth of the spray-containing region during shear breakup.

which implied that drops produced by breakup had diameters comparable to the thickness of this liquid viscous region.

(4) The parent drop accelerates rapidly due to the large drag coefficient caused by its deformation; a phenomenological analysis provided an effective correlation of the resulting parent drop velocities.

(5) The mean velocities of drops produced by shear breakup at small Ohnesorge numbers were relatively independent of drop size, and were somewhat larger than the velocities of the parent drop, at each instant of time.

(6) The rms velocity fluctuations of drops produced by shear breakup at small Ohnesorge numbers were relatively independent of drop size, and were on the order of 30–40% of the mean streamwise velocity of the gas relative to the parent drop, at each instant of time.

(7) The rate of liquid removal from the parent drop could be interpreted reasonably well based on the variations of parent drop diameter and the size and velocity of drops leaving the periphery of the parent drop; these results were correlated concisely in terms of an empirical clipped Gaussian function.

(8) Shear breakup at small Ohnesorge numbers extends over streamwise distances of 0–100 initial drop diameters, and 0–5.5 characteristic drop breakup times; this behavior suggests that shear breakup should be treated as a rate process, rather than by jump conditions, in some instances.

Acknowledgements—This research was sponsored by the Air Force Office of Scientific Research Grant Nos. F49620-92-J-0399 and F49620-95-1-0364, under the technical management of J. M. Tishkoff. The authors would like to thank C. W. Kauffman for the loan of the shock tube facility and advice concerning its operation. The U.S. Government is authorized to reproduce and distribute copies of this article for governmental purposes notwithstanding any copyright notation thereon.

REFERENCES

Belz, M. H. (1973) *Statistical Methods in the Process Industries*, pp. 103–104. Wiley, New York.

Clift, R., Grace, J. R. and Weber, M. E. (1978) *Bubbles, Drops and Particles*, pp. 26 and 339–347. Academic Press, New York.

Dabora, E. K. (1967) Production of monodisperse sprays. *Rev. Scient. Instrum.* **38,** 502–506.

Faeth, G. M. (1990) Structure and atomization properties of dense turbulent sprays. In *Proc. 23rd Symp. (Int.) on Combustion*. The Combustion Institute, Pittsburgh, PA, pp. 1345–1352.

Faeth, G. M. (1996) Spray combustion phenomena. In *Proc. 26th Symp. (Intl) on Combustion*, The Combustion Institute, Pittsburgh, PA, in press.

Giffen, E. and Muraszew, A. (1953) *The Atomization of Liquid Fuels*. Chapman & Hall, London.

Hanson, A. R., Domich, E. G. and Adams, H. S. (1963) Shock-tube investigation of the breakup of drops by air blasts. *Phys. Fluids* **6,** 1070–1080.

Hinze, J. O. (1955) Fundamentals of the hydrodynamic mechanism of splitting in dispersion processes. *AIChE J.* **1,** 289–295.

Hsiang, L.-P. and Faeth, G. M. (1992) Near-limit drop deformation and secondary breakup. *Int. J. Multiphase Flow* **18,** 635–652.

Hsiang, L.-P. and Faeth, G. M. (1993) Drop properties after secondary breakup. *Int. J. Multiphase Flow* **19,** 721–735.

Hsiang, L.-P. and Faeth, G. M. (1995) Drop deformation and breakup due to shock wave and steady disturbances. *Int. J. Multiphase Flow* **21,** 545–560.

Krzeczkowski, S. A. (1980) Measurement of liquid droplet disintegration mechanism. *Int. J. Multiphase Flow* **6,** 227–239.

Lane, W. R. (1951) Shatter of drops in streams of air. *Ind. Engng Chem.* **43,** 1312–1317.

Lange, N. A. (1952) *Handbook of Chemistry*, 8th edn, pp. 1134 and 1709. Handbook Publishers, Inc., Sandusky, OH.

Liang, P. Y., Eastes, T. W. and Gharakhari, A. (1988) Computer simulations of drop deformation and drop breakup. AIAA Paper No. 88-3142.

Loparev, V. P. (1975) Experimental investigation of the atomization of drops of liquid under conditions of a gradual rise of the external forces. *Izvestiya Akad. Nauk SSSR, Mekh. Zhidkosti i Gaza* **3,** 174–178.

Ranger, A. A. and Nicholls, J. A. (1969) The aerodynamic shattering of liquid drops. *AIAA J.* **7,** 285–290.

Reinecke, W. G. and McKay, W. L. (1969) Experiments on waterdrop breakup behind Mach 3 to 12 shocks. Sandia Corp. Report SC-CR-70-6063.

Reinecke, W. G. and Waldman, G. D. (1970) A study of drop breakup behind strong shocks with applications to flight. Avco Report AVSD-0110-70-77.

Sangiovanni, J. and Kestin, A. S. (1977) A theoretical and experimental investigation of the ignition of fuel droplets. *Combust. Sci. Technol.* **6,** 59–70.

Schlichting, H. (1975) *Boundary Layer Theory*, 7th edn, pp. 234–235 and 599. McGraw-Hill, New York.

Simmons, H. C. (1977) The correlation of drop-size distributions in fuel nozzle sprays. *J. Engng Power* **99,** 309–319.

White, F. M. (1974) *Viscous Fluid Flow*. McGraw-Hill, New York.

Wierzba, A. and Takayama, K. (1987) Experimental investigations on liquid droplet breakup in a gas stream. *Report Inst. High Speed Mech.*, Tohoku Univ., Vol. 53, No. 382, pp. 1–99.

Wierzba, A. and Takayama, K. (1988) Experimental investigation of the aerodynamic breakup of liquid drops. *AIAA J.* **26,** 1329–1335.

Wu, P.-K., Ruff, G. A. and Faeth, G. M. (1991) Primary breakup in liquid/gas mixing layers for turbulent liquids. *Atom. Sprays* **1,** 421–440.

Wu, P.-K., Hsiang, L.-P. and Faeth, G. M. (1995) Aerodynamic effects on primary and secondary breakup. *Prog. Astro. Aero.* **169,** 247–279.